

# Evolution of pitch angle distributions of relativistic electrons during geomagnetic storms: Van Allen Probes Observations

Ashley D. Greeley<sup>1</sup>, Shrikanth G. Kanekal<sup>1</sup>, David G. Sibeck<sup>1</sup>, Quintin Schiller<sup>2</sup>, Daniel N. Baker<sup>3</sup>

<sup>1</sup>NASA Goddard Space Flight Center, Greenbelt, MD, USA

<sup>2</sup>Space Science Institute, Fort Atkinson, WI, USA

<sup>3</sup>Laboratory for Atmospheric and Space Physics, University of Colorado Boulder, Boulder, CO, USA

## Key Points:

- The evolution of electron pitch angle distributions can be tracked well by a pitch angle index, 'n' in  $J_0 \sin^n \theta$
- Ultra relativistic electrons consistently have a higher n than relativistic electrons
- Isotropization rates can be linearly fit and statistically differ between CME- and CIR-driven storms

## Abstract

We present a study analyzing relativistic and ultra relativistic electron energization and the evolution of pitch angle distributions using data from the Van Allen Probes. We study the connection between energization and isotropization to determine if there is a coherence across storms and across energies. Pitch angle distributions are fit with a  $J_0 \sin^n \theta$  function, and the variable 'n' is characterized as the pitch angle index and tracked over time. Our results show that, consistently across all storms with ultra relativistic electron energization, electrons become most anisotropic within around a day of  $Dst_{min}$  and relax down to prestorm isotropization levels in the following week. In addition, each consecutively higher energy channel is associated with higher anisotropy after storm main phase. Changes in the pitch angle index are reflected in each energy channel; when 1.8 MeV electrons increase (or decrease) in pitch angle index, so do all the other energy channels. In a superposed epoch study, we show that the peak anisotropies differ between CME- and CIR- driven storms and measure the relaxation rate as the anisotropy falls after the storm. The relaxation rate in pitch angle index for CME-driven storms is  $-0.14 \pm 0.023$  at 1.8 MeV,  $-0.28 \pm 0.01$  at 3.4 MeV, and  $-0.36 \pm 0.02$  at 5.2 MeV. For CIR-driven storms, the relaxation rates are  $-0.09 \pm 0.01$  for 1.8 MeV,  $-0.12 \pm 0.02$  for 3.4 MeV, and  $-0.11 \pm 0.02$  for 5.2 MeV. This study shows that there is a global coherence across energies and that storm type may play a role in the evolution of electron pitch angle distributions.

## Plain Language Summary

Using Van Allen Probes data, we measure pitch angle distributions of relativistic and ultra relativistic electrons. Anisotropic pitch angle distributions are sharply peaked around 90 degrees. More evenly distributed pitch angles are isotropic. Our results show that, consistently across all storms with ultra relativistic electron enhancements, electrons become most anisotropic within around a day of storm onset and slowly isotropize in the following week. In addition, each consecutively higher energy channel is also associated with higher anisotropy after the main phase of geomagnetic storms, a characteristic which holds through the storm and recovery. Changes in the pitch angle index are reflected in each energy channel; when 1.8 MeV electrons increase (or decrease) in pitch angle index, so do all the other energy channels. In a superposed epoch study, we show that the peak anisotropies differ between different storm drivers (namely, coronal mass ejections and corotating interaction regions) and measure the relaxation rate as the anisotropy falls after the storm. This study shows that there is a global coherence across energies and that storm type may play a role in the evolution of electron pitch angle distributions.

## 1 Introduction

In the recent past, several space missions, including the Van Allen Probes (Mauk et al., 2013; D. Sibeck et al., 2012) and Arase (“Geospace exploration project ERG”, 2018), have provided detailed observations of the Earth’s radiation belts. They have not only revealed new phenomena (Baker et al., 2013), but also advanced our understanding of dynamics of electron energization and loss in the radiation belts. Both radial diffusion and wave-particle interactions (Baker et al., 2014; G. D. Reeves et al., 2013) lead to energization and loss of electrons in the outer Van Allen belt.

The importance of wave-particle interactions in both energizing and pitch angle scattering electrons is now well established. Chorus wave driven in-situ energization and subsequent ULF wave driven radial diffusion result in energization to relativistic and ultra-relativistic electrons (O’Brien et al., 2003; Claudepierre et al., 2008; Mourenas et al., 2014). Recent observations have shown direct evidence of pitch angle scattering (Fennell et al., 2014; Kasahara et al., 2018) as well as provided a comprehensive survey of energization

time scales and associated wave phenomena (Baker et al., 2014). Observations have also shown cross-scale coupling between the lowest and highest energy electron populations. Low energy electrons have a pitch angle anisotropy which leads to wave generation, which in turn acts upon a “seed” population of “intermediate” energies, accelerating them to relativistic energies (Jaynes et al., 2015). Theoretical studies and modeling provide a robust frame-work for understanding the physical processes for the role of various plasma waves affecting electron dynamics (Summers et al., 1998; Thorne et al., 2013, 2013).

Despite the observational and theoretical advances, there are aspects of physical processes that drive the energization and loss which are not completely understood; for example the connection between pitch angle scattering, i.e., flux isotropization and electron enhancement has not been explored in detail. Early studies (G. Reeves et al., 1998) suggested that electrons with large pitch angles  $\sim 90^\circ$  are energized first, followed by isotropization. However, subsequent studies seemed to suggest that energization and isotropization were nearly simultaneous (Kanekal, 2006; Kanekal et al., 2005, 2001). These early studies were limited by insufficient temporal resolution (Kanekal et al., 1999), limited L coverage (Kanekal et al., 2001), and the use of multiple spacecraft in different orbits.

In this study, we use Van Allen Probes measurements to examine the relationship between electron energization and pitch angle distributions (PAD) during electron enhancements. We also analyze events driven by coronal mass ejections (CMEs) and corotating interaction regions (CIRs) separately. We perform superposed epoch analysis on the PAD evolution of relativistic and ultra-relativistic electron enhancements for 20 CME- and 24 CIR-driven events. The near-equatorial orbit of Van Allen Probes allows for large pitch angle coverage and the Relativistic Electron Proton telescope (REPT) measures electrons over a wide energy range with excellent pitch angle coverage (see Section 2).

PADs appear within the radiation belts in several distinctive shapes. These shapes are created by different mechanisms, such as wave-particle interactions or radial diffusion. Three common types of PADs are pancake, butterfly, and flat top (Chen et al., 2014). “Pancake” PADs peak at  $90^\circ$  and are thought to be caused by inward radial diffusion (Zhao et al., 2018) and/or wave-particle interactions (Ni et al., 2015). They are most prominent on the dayside (Gannon et al., 2007; West Jr. et al., 1973). The sharper the peak at  $90^\circ$ , the more anisotropic the PADs are. “Butterfly” distributions exhibit peak fluxes at  $45^\circ - 60^\circ$  pitch angles and lower fluxes near- $90^\circ$  pitch angles, and could be caused by drift shell splitting (Stone, 1963) with or without magnetopause shadowing (Selesnick & Blake, 2002; D. G. Sibeck et al., 1987) in the outer belt. “Flat top” distributions have low fluxes at  $0^\circ$  and  $180^\circ$  and are flat over a range of pitch angles around  $90^\circ$ . These are considered isotropic. They could be a result of a transition between pancake and butterfly distributions, or could result from wave-particle interactions (Horne et al., 2003). Other types of pitch angle distributions can exist, but are less common (Zhao et al., 2018; Baker et al., 1978; D. G. Sibeck et al., 1987). Understanding the evolution of pitch angle distributions of different energetic populations, and the drivers that affect them, are essential to understand radiation belt physics.

Section 2 gives details regarding the instrument and spacecraft used in this study. The methods used to track pitch angle distributions over time are in Section 3. Results from single storm analysis and a statistical study are shown in Section 4. Section 5 contains a discussion on the results presented, and we conclude with a summary in Section 6.

## 2 Spacecraft and Data

This study uses data from NASA’s Van Allen Probes mission (Mauk et al., 2013), consisting of two satellites launched in 2012 into a highly elliptical orbit ( $\sim 500$  to  $30,000$  km). Both identically instrumented spacecraft have sunward-pointing spin axes and spin

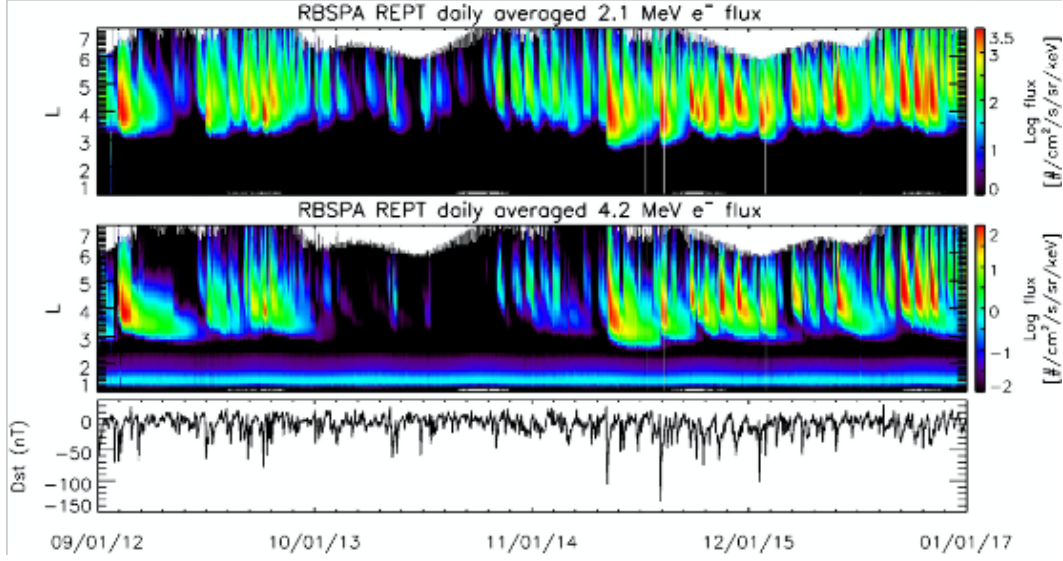


**Figure 1.** Lsort plots from RBSPA REPT channels from 2012-2017. The top panel is 2.1 MeV electrons and the bottom panel represents 4.2 MeV electrons. The bottom panel shows Dst index. This figure is adapted from Zhao et al. (2018)

at  $\sim 6$  rotations per minute (RPM) in the near-equatorial region at  $10^\circ$  inclination, allowing for broad sampling of pitch angles. They each carry five instrument suites to measure electrons, ions, plasma waves, and magnetic and electric fields. By using two spacecraft, the spatial and temporal extent of various phenomena can be measured. One laps the other every several months, allowing for a wide range of spatial measurements. The prime mission lifetime for Van Allen Probes was two years, but both spacecraft collected data for over seven years. The Van Allen Probes mission was launched near the peak of solar cycle 24, during which coronal mass ejections (CMEs) are more frequent, and covered the declining phase (mid-2014 through end of mission), when CIR/HSS are the dominant solar drivers.

The REPT instrument onboard the Van Allen Probes is a particle telescope comprising a stack of silicon solid-state detectors (SSDs) enclosed in aluminum-tungsten shielding. REPT measures charged electrons and protons with a geometry factor of  $0.2 \text{ cm}^2\text{sr}$  (Baker et al., 2012). It measures electrons  $\sim 2\text{-}20 \text{ MeV}$  in 8 differential energy channels with an energy resolution  $\Delta E/E$  of 30%. We can therefore observe PAD changes from the relativistic to ultra relativistic energy regime using a single instrument. Van Allen Probes passes through the inner and outer belts during its orbit, and maps both these regions well over long periods of time.

Figure 1, adapted from Figure 2 of Zhao et al. (2018), shows REPT long-term Lsort plots from the 2.1 and 4.2 MeV electron energy channels, spanning 2012-2017. The bottom panel shows Dst index for this time period. The flux is color coded where red is the most intense flux and black is close to zero. Enhancements occur more frequently in the 2.1 MeV energy channel, electrons are less frequently energized to ultra relativistic energies.

### 3 Determining Pitch Angle Index

In this paper, we describe the characterization of pitch angle distributions of relativistic and ultra relativistic electrons in the REPT instrument and track this distri-

bution over time. We will use this data to determine if there is a coherence in PAD changes across energies, if there is a pattern across storms, and if storm driver affects the pitch angle distribution of the electrons. To do so, we must first select time periods of enhanced relativistic and ultra relativistic electrons.

During 2012-2018, Zhao et al. (2019) found that REPT only observes  $>5.2$  MeV electrons after a geomagnetic storm, and, further, that all REPT electrons were more likely to be enhanced after a storm of any size. Since REPT energy channels start at 1.8 MeV, the instrument exclusively measures relativistic and ultra relativistic electrons. Therefore, in order to study pitch angle distributions of electron populations up to ultra relativistic energies, we look for electron enhancements after geomagnetic storms. Around half of geomagnetic storms result in relativistic electron enhancements (G. D. Reeves et al., 2003).

In order to find storms with electron enhancements, we first selected days where the  $Dst$  index dropped below -40 nT and evaluated these time periods for ultrarelativistic enhancements. Following a method by Turner et al. (2015), we compared the maximum flux in each energy channel between 12 and 84 hours after the  $Dst_{min}$  to the maximum flux between 12 and 84 hours before the  $Dst_{min}$ . Electrons in a given energy channel are considered to be enhanced if the poststorm maximum flux is at least twice the prestorm maximum flux. There may only be flux enhancements in some energy channels, and indeed, we find that lower electron energy channels are more likely to be enhanced following a geomagnetic disturbance, in agreement with Zhao et al. (2019). We selected storms that result in an electron enhancement in at least the REPT 1.8, 2.1, 2.6, and 3.4 MeV electron channels.

Next, we determined the likely storm driver, using OMNI data (available on CDAweb at <https://cdaweb.sci.gsfc.nasa.gov>) to plot storm characteristics, such as solar wind velocity, proton temperature in the solar wind, AE index, IMF  $B_z$ , and SYM-H. CME-driven storms tend to have abrupt changes in AE,  $B_z$ , solar wind flow speed, and an increase in proton temperature shortly after storm commencement (Neugebauer & Goldstein, 2013). A CIR-driven storm tends to exhibit slower variations - solar wind velocity slowly increases, proton temperature in the solar wind may reach its max before storm commencement, and  $Dst$  (or SYM-H) index may be less intense and vary more during recovery (Jian, 1993). In addition, in a CIR-driven storm,  $B_z$  may fluctuate more, whereas in a CME-driven storm there is more often one a sudden drop. Not every storm will have each of these indicators, but together, they may point to the likely source of a geomagnetic storm. We corroborated our results from published storm lists as much as possible (Richardson & Cane, 2019; Shen et al., 2017; Bingham et al., 2018), and found them to be consistent with our categorization.

Pitch angle distributions within the radiation belts change as a function of L (Gannon et al., 2007), so choosing the L location in which to track pitch angle distributions is important. We want to track the pitch angle distribution of the enhanced electrons, therefore we select an L band where there is maximum electron intensity in the outer belt. The L band extent must be optimized. On one hand, the L range cannot be too narrow, because the enhanced electrons drift inwards over the course of several days, and an overly narrow L range would lose important information regarding the enhanced population. On the other hand, attempting to fit the average pitch angle distribution over a very large L bin smooths out interesting features. We selected a bin size of 0.8 L centered around the average max flux during the 5 days after Dst minimum to balance out these concerns. Neither shifting nor changing the size of the bin by several tenths of an L changed the results of the analysis.

We obtained the average unidirectional differential electron flux (FEDU) for each energy channel, within the L range of interest, and in  $10^\circ$  pitch angle bins. Then, we interpolated over pitch angle and fit the distribution with the functional form  $J_0 \sin^n \theta$  be-

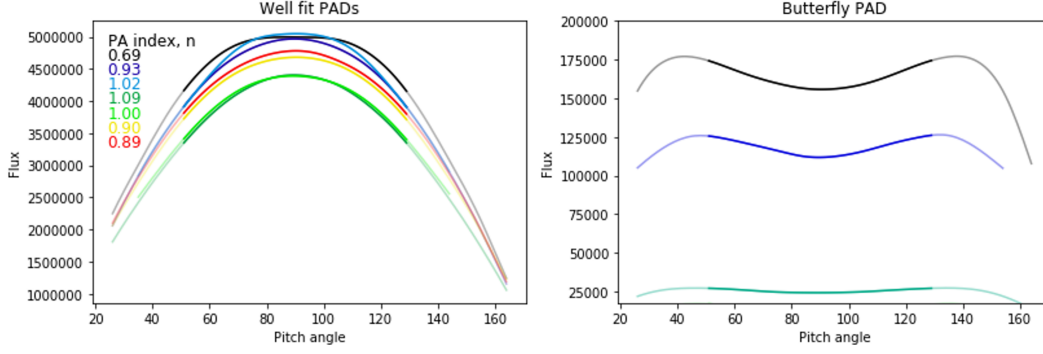


**Figure 2.** Example pitch angle distributions from REPT data in the 1.8 MeV electron bin. Plot on the left shows pitch angle distributions that are well fit to a  $\sin^n\theta$  function. The color of each pitch angle distribution is associated with a pitch angle index, 'n', from the fit to the data. The pitch angle index is shown to the left. The right plot shows a few examples of pitch angle distributions that the algorithm determined to be a butterfly pitch angle distribution. For each plot, the more saturated lines show where the data was fit.

tween 50 and 130 degrees. Within this equation, 'n' is defined as the pitch angle index, as it will be referred to from this point on. The  $\chi^2$  value from the fit is calculated as

$$\chi = \sum \frac{(y - fit)^2}{(0.0002)y^2} \quad (1)$$

which assumes a systematic error of about 1%. The statistical errors on flux measurements are small compared to systematic errors. This is then divided by degree of freedom (77) to find the  $\chi^2$  per degree of freedom. Pitch angle distribution fits with a  $\chi^2/\text{d.o.f} > 4$  are discarded.

Butterfly pitch angle distributions are not well fit with a  $\sin^n\theta$  function, and are excluded from the study. Following the method outlined in Zhao et al. (2014),

$$edge_{values} = f_{avg}(90^\circ - \alpha : 90^\circ + \alpha) \quad (2)$$

is calculated for values of  $\alpha$  from  $5^\circ$  to  $45^\circ$ . The max of these 'edge values', multiplied by 0.95, is compared to the mean flux of  $85^\circ$ – $95^\circ$  ('middle values'). If the middle values are lower than the edge values, it is flagged as a butterfly distribution. Butterfly PADs most commonly result from drift shell splitting, which is more pronounced at high L shells (D. G. Sibeck et al., 1987). The average L range in this study is 3.9–4.7, so butterfly PADs are not a significant portion of the distribution types, particularly at the lower energy channels. In the discussion section, we discuss the butterfly occurrences found during storms with enhancements.

Figure 2 shows a few examples of REPT pitch angle distributions. The panel on the left shows 7 PADs that are well fit to the  $\sin^n\theta$  function. The color of each distribution is associated with its pitch angle index, shown to the left. The pitch angle index gives a numerical value the the anisotropy of the PAD. The pitch angle index does not take flux into account. The panel on the right shows 3 examples of butterfly distributions selected by our algorithm. These are excluded from the analysis. In both plots, the full PAD is shown in a light color, with the fit range in a more saturated color.

Pitch angle distributions that can be fit well with  $J_0 \sin^n\theta$  were compiled into a database. For each geomagnetic storm, there was a time series of pitch angle indices for each electron energy channel containing an enhancement. Within each selected storm, we study



PADs of electrons covering a range of energies to determine if there is a coupling from relativistic ( $\sim 1$  MeV) to ultra relativistic ( $> 3$  MeV) energies by comparing the pitch angle index for energy channels over time. In addition, we compare PADs between storms to determine if there are similarities across storms, as well as storms grouped by solar drivers, i.e., CMEs and CIRs.

## 4 Results

### 4.1 Individual Storm Analysis

Firstly, we track the pitch angle index over time in each enhanced energy channel during individual storms. By analyzing a single storm at a time, it is possible to determine if there are any patterns across energy channels.

Figure 3 shows combined results from REPT probe A and B from a storm on June 29, 2015. The first three panels show electron flux as a function of L and time, color coded as shown in the color bars to the right of each panel. From top to bottom, the energy channels are 1.8, 3.4, and 7.7 MeV. The black dots indicate the location of maximum flux in L over each orbital pass. The L range analyzed in this storm was 3.4-4.2 L. Panel (d) shows pitch angle index, 'n', as a function of time for electron energies ranging from 1.8 to 6.3 MeV. Energy channels are shown in different colors, from cool (purple, at 1.8 MeV) to warm (red, at 6.3 MeV). There were no pitch angle indices from 7.7 MeV, as the analyzed unidirectional fluxes were not large enough to fit well to the  $J_0 \sin^n \theta$  distribution. The error from the fit are shown as pitch angle index errors. The bottom panel (e) shows  $Dst$  (nT) for the duration of the storm. Vertical lines show the time of minimum  $Dst$ .

The 1.8 MeV energy channel has a pitch index for every time the spacecraft travels through the outer belt. At higher energies, there are some gaps in the data. The gaps in pitch angle index for various energies are due to either low flux levels, high  $\chi^2$  value of the pitch angle distribution fit, or due to a measured butterfly distribution. The MLT of the data points are shown as a second x axis, and this particular plot is only for inbound passes of Van Allen Probes. The pitch angle distributions of the outer belt can vary over MLT, so we divided storms into inbound and outbound passes to be able to compare populations more directly within storms. These pitch angle indices are from the afternoon sector.

Before the  $Dst_{min}$ , pitch angle indices for all energy bins were low, specifically less than 2 for all energy channels. This means that the pitch angle distributions were fairly isotropic. When the storm compressed the magnetosphere and the seed population energized, the resulting enhanced electrons are very anisotropic. The higher the energy channel, the more anisotropic the pitch angle distributions are. The pitch angle indices peak within about one day of  $Dst_{min}$  and decrease until July 6, when there is another large drop in  $Dst$ . The highest energy electrons show up (at measurable values) within a few days of  $Dst_{min}$ .

Figure 4 shows the pitch angle index evolution for another storm, this one in March, 2019. The panels and markers are the same as in Figure 3. In this storm, the enhancement can only be measured up to the 5.2 MeV energy channel, and there appears to be a second peak in the pitch angle index around 2 days after  $Dst_{min}$ . The higher energy electron channels are also associated with consistently higher anisotropies, and the patterns across energies are the same as for the previous storm.

These plots show just 2 of the 43 storms analyzed for this study, but the qualitative characteristic of all of the storms are similar. In each of the storms analyzed, the characteristics of electron PADs during enhancement or energization evolve in a similar manner. When the pitch angle indices increased, they did so at every observed en-

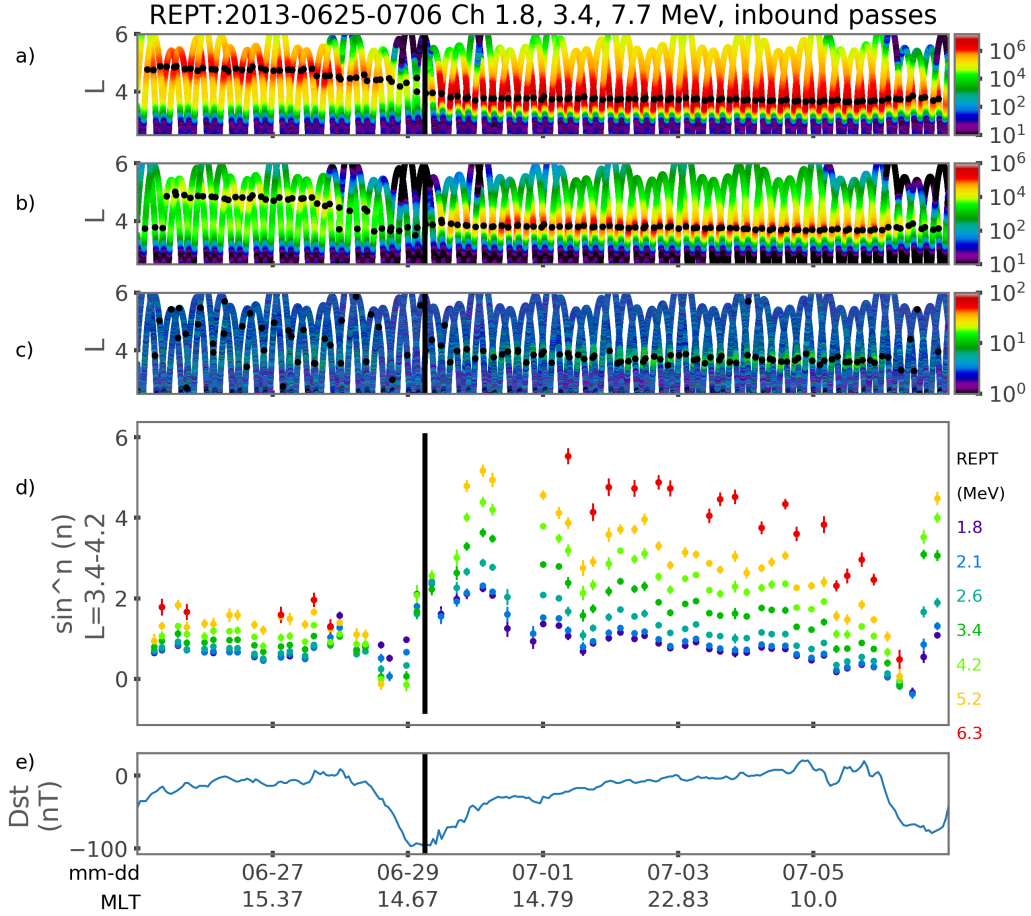


**Figure 3.** Fluxes of 1.8, 3.4, and 6.3 MeV electrons as a function of L (top three panels), color coded by flux, shown in the right for a storm on June 29, 2013. Black dots indicate the location in L of the flux maximum at each pass of the spacecraft through the outer belt. The fourth panel (d) shows pitch angle index ( $n$ ) values for inbound passes of A and B. The bottom panel (e) shows the  $Dst$  index. Vertical black line indicates time of  $Dst_{min}$ , and MLT is shown as a second x-axis.



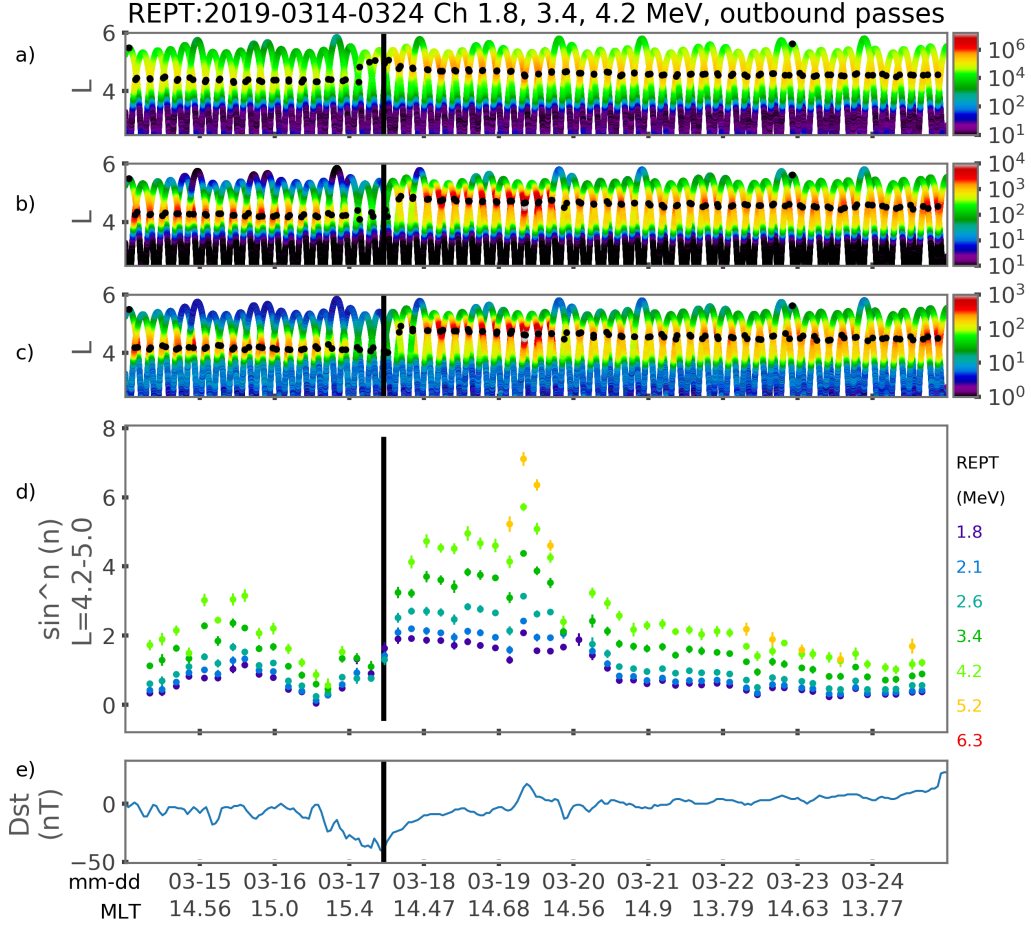


**Figure 4.** Fluxes of 1.8, 3.4, and 6.3 MeV electrons as a function of  $L$  (top three panels), color coded by flux, shown in the right for a storm on March 17, 2019. Black dots indicate the location in  $L$  of the flux maximum at each pass of the spacecraft through the outer belt. The fourth panel (d) shows pitch angle index ( $n$ ) values for inbound passes of A and B. The bottom panel (e) shows the  $Dst$  index. Vertical black line indicates time of  $Dst_{min}$ , and MLT is shown as a second x-axis.

ergy. A decrease in pitch angle index was similarly reflected across energy channels. This occurred for every time step within every storm. There is a clear coherence between relativistic and ultra relativistic enhancements. The changes that occur in tandem do so within the resolution of one orbital pass of Van Allen Probes, viz.,  $\approx 5$  hours. In addition, the pitch angle index consistently increases with energy, i.e., the higher energy channels (6.3 MeV) are always associated with a higher pitch angle index than lower energy channels (1.8 MeV).

## 4.2 Superposed Epoch Study

Next, we investigate the average evolution of pitch angle distributions associated with electron energization. We will show that the pitch angle distributions of energized electrons change in the same manner over time for different storms. We conducted superposed epoch studies comparing evolution of electron PADs during CME-driven storms and CIR-driven storms. We found that there was a clear distinction between the pitch angle distribution evolution for different storm drivers.

We analyzed 20 CME- and 23 CIR-driven Van Allen Probes era storms with ultra relativistic enhancements. For each energy channel, the pitch angle indices were averaged in bin sizes of half a day, weighted by the error on their fit. The superposed epoch error was calculated as the relative error summed in quadrature. Bins with fewer than 1/5 of the total storms are not shown.

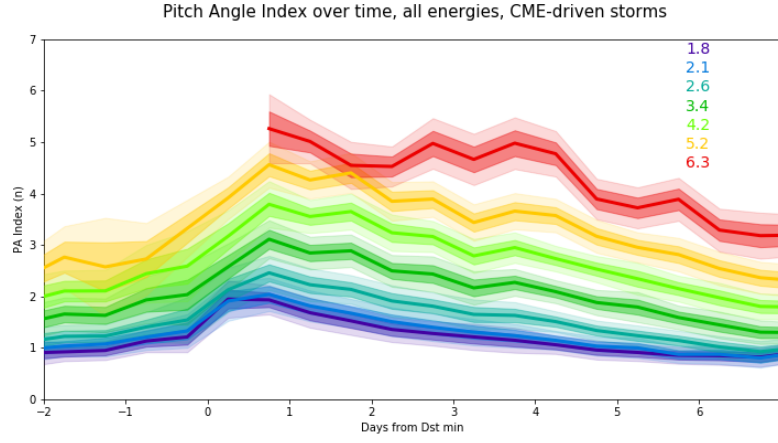
Figure 5 shows the resulting superposed epoch plot for CME-driven storms only, with electron energies ranging from 1.8-6.3 MeV. Figure 6 shows the superposed epoch plot for CIR-driven storms. Both Figure 5 and Figure 6 show superposed epoch curves for each energy in different colors (as indicated in the plot). For each energy, the thin darkest line is the weighted average pitch angle index ( $n$ ), with 1 sigma and 2 sigma errors shown as shaded regions around the mean.

The pitch angle indices for CME-driven storms peak higher than CIR-driven storms. At 1.8 MeV, pitch angle indices ( $n$ ) are 1.80 and 1.94 for CIR and CME-driven storms, respectively, and, similarly, 4.60 and 5.26 for 6.3 MeV electrons. CME-driven storms overall have a greater pitch angle distribution anisotropy in the day after  $Dst_{min}$  at relativistic and ultra relativistic energies.

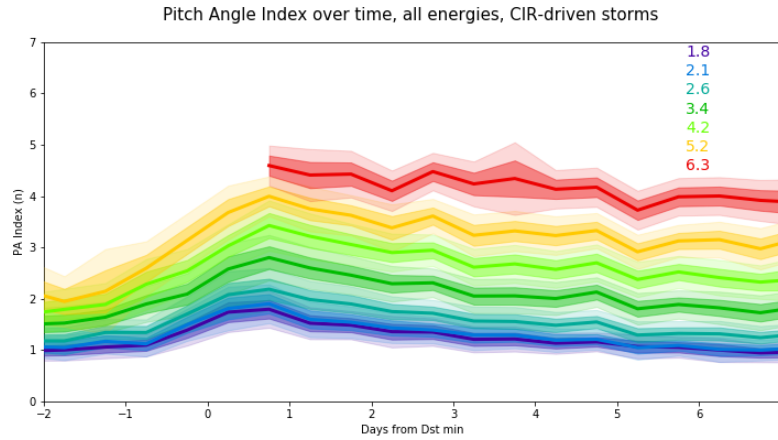
We analyzed the isotropization rate from peak anisotropy until 7 days after  $Dst_{min}$ . This was done for the superposed epoch of each energy channel and storm driver to determine how the average rate is different in each of these situations. The isotropization rate is well fit to a linear function.

Figure 7 compares the electron pitch angle indices for the 1.8, 3.4, and 5.2 MeV energy channels in CME- and CIR-driven storms and shows a linear fit to the isotropization rate of each energy. The figure shows superposed epoch curves corresponding to each energy in dark(light) colors for CME(CIR)-driven storms. The electron energy channels and solar driver types are indicated in the legend on the plot. The isotropization of the pitch angle distributions is quantified by fitting the slope of the pitch angle distribution evolution for each of the electron energy bins for CME- and CIR-driven storms. The slopes and standard error on the slope is shown in the legend. The relaxation rate for CME-driven storms is  $-0.14 \pm 0.023$  at 1.8 MeV,  $-0.28 \pm 0.01$  at 3.4 MeV, and  $-0.36 \pm 0.02$  at 5.2 MeV. For CIR-driven storms, the relaxation rates are  $-0.09 \pm 0.01$  for 1.8 MeV,  $-0.12 \pm 0.02$  for 3.4 MeV, and  $-0.11 \pm 0.02$  for 5.2 MeV in pitch angle index units per day.

From Figure 7, it is evident that the anisotropy in pitch angle distribution occurs within a day for both CME- and CIR-driven storms, but that the scale on which they occur is not the same. CIR-driven storms tend to exhibit slightly lower pitch angle anisotropies.



**Figure 5.** Superposed epoch study of PAD evolution for 20 CME-driven storms for energies 1.8-6.3 MeV. Color lines show weighted average PA index evolution, with lighter 1 sigma and 2 sigma error around the mean.



**Figure 6.** Superposed epoch study of PAD evolution for 23 CIR-driven storms for energies 1.8-6.3 MeV. Color lines show weighted average PA index evolution, with lighter 1 sigma and 2 sigma error around the mean.

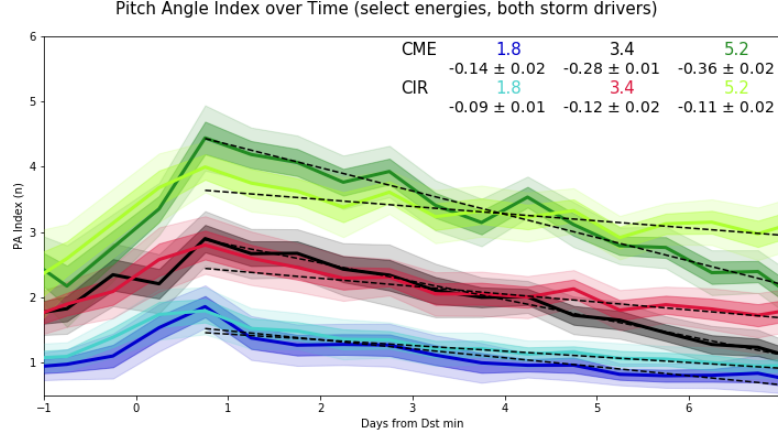


**Figure 7.** Superposed epoch study of PAD evolution for electrons of energies 1.8, 3.4, and 5.2 MeV, for CME- and CIR-driven storms. CME(CIR) curves are shown in dark(light) colors. The CIR-driven storms are shown in light blue, red, and light green, and CME-driven storms are shown in dark blue, black, and dark green. The superposed epoch curve is shown as a solid line with shaded bands showing the 1 sigma error.

This is true for the relativistic (1.8 MeV) and ultra relativistic (3.4 and 5.2 MeV) electrons. A clear energy dependence is seen in the rate at which PADs isotropize for CME-driven storms, and the isotropization rate more than doubles between the 1.8 and 5.2 MeV energy bins. The isotropization rates for CIR-driven storms changes between energy channels, but there is not a clear energy dependence. The isotropization rate for CME-driven storms is higher than the CIR-driven storms in each energy channel, but it diverges the most at higher energies. The slopes are statistically different for each energy channel.

## 5 Discussion

The individual storm analysis results show that relativistic and ultra relativistic electrons are associated with strong anisotropies soon after storm main phase. In addition, we found that between any two energy channels, the higher energy electrons are more anisotropic than the lower energy electrons during every storm with enhancements analyzed. Relativistic and ultra relativistic electrons are either energized around  $90^\circ$  or energize isotropically and quickly anisotropize after energization due to strong pitch angle diffusion into the loss cone. We cannot differentiate between the two when instrument measurements are many hours apart.

Previous studies have found that wave-particle interactions are most effective at accelerating relativistic energy electrons (Thorne, 2010). More recently, studies have shown that a combination of wave-particle interactions and radial diffusion can be an effective acceleration combination during geomagnetic storms (Zhao et al., 2019; Jaynes et al., 2018). Jaynes et al. (2018) found that ULF wave acceleration followed by inward radial diffusion can energize source populations to ultra relativistic energies. Electrons with pitch angles near  $90^\circ$  are more effectively energized by radial diffusion (Chen et al., 2007; Lejosne & Kollmann, 2020), which may explain the anisotropies of the higher energy electrons, and why pitch angles appear to become more anisotropic on similar timescales. This is consistent with our results, which show the most anisotropy at the highest energies in the day after Dst minimum.

From our results, it is evident that pitch angle distributions also isotropize on similar time scales across a wide range of energies. Wave-particle interactions via cyclotron resonance may not be able to interact with electrons from relativistic all the way to ultra relativistic energies. For example, the effect of EMIC waves on precipitation via cyclotron resonance is well studied (Jordanova et al., n.d.; Summers & Thorne, 2003). The EMIC wave minimum resonance energy for cyclotron resonance is most often above  $\sim 2$  MeV (Meredith et al., 2003; Summers & Thorne, 2003), so would be unable to account for isotropization in all observed REPT energy channels. However, if other types of resonances are considered, such as Landau or bounce, the energy range affected broadens dramatically and may in fact play a dominant role in the isotropization rates of energetic electrons.

More recent results from Fu et al. (2018) show that quasilinear Landau resonance interactions are less likely to cause precipitation, but can pitch angle scatter near equatorial electrons to lower pitch angles. This is especially striking due to its effectiveness across a wide range of energies, from 10s of keV to 10 MeV. Another recent study shows that nonlinear Landau trapping can effectively pitch angle scatter energetic electrons from  $89^\circ$  to  $80^\circ$  in a matter of seconds (Wang et al., 2016). They showed effective scattering results from 10 keV to 5 MeV, but did not test the upper energy limit, so this scattering may continue to even higher energies.

Chorus waves and hiss have also been shown to have non cyclotron resonant interactions that can affect a wide range of energetic electrons. Chorus waves may affect the second adiabatic invariant, and scatter relativistic electrons near the equator (Shprits, 2009). Fu et al. (2020) shows that in addition, hiss can bounce and Landau resonate with equatorial pitch angles. They claim that hiss may be an important mechanism in the evolution of pitch angle distributions. Ultimately, there may be a variety of waves that can interact with relativistic and ultra relativistic electrons via Landau and bounce resonances. Our results indicate that these types of interactions may dominate during and after geomagnetic storms. The connection between effective pitch angle scattering and Landau resonance would be an interesting future topic.

We can also draw the following conclusions from the superposed epoch analysis of pitch angle index changes. For all storm drivers, pitch angle distributions are most anisotropic within one day after Dst minimum. Subsequently, the pitch angle distributions isotropize over time, but at different rates, depending on the storm driver. This result agrees with and furthers the work of other studies, which qualitatively state that pitch angle distributions isotropize after storms (Lyons & Williams, 1975; Ni et al., 2015). This isotropization could mean that either electrons diffuse in pitch angle faster during CME-driven storms, or there are continual injections at large pitch angles during CIR-driven storms that affect the overall distribution shape.

Two potential limitations of our study are due to butterfly pitch angle distributions and pitch angle distribution differences due to the Van Allen Probes orbit traversing a range of magnetic latitude. Butterfly distributions are poorly fit with a  $\sin^n\theta$  function, and are not easily labeled as 'anisotropic' or 'isotropic.' However, we found that, overall, the number of butterfly PADs was relatively small. In the five days after *Dst* minimum, butterfly PADs made up  $< 2\%$  of the total number of fits in the 1.8-4.2 MeV electron energy channels. They accounted for  $\sim 4\%$  of the fits in the 5.2 MeV channel, but at 6.3 MeV they made up almost 25% of the fits. The analysis in this study focuses on the 1.8-5.2 MeV electrons, thus the butterfly PADs do not significantly affect our results.

The magnetic latitude of the spacecraft can affect PAD, making them appear more anisotropic off the equator than equatorial measurements would show. Zhao et al. (2014) found that pitch angle distributions as little as 10 degrees off the equator could affect the distribution measurement. However, in our superposed epoch analysis, restricting  $|\text{MLAT}|$  to  $< 5^\circ$  did not alter the relaxation rates greater than the fit error. In addi-

tion, the results from the single storm analyses are qualitative and would not be affected by small changes in the pitch angle index. Even if some of the pitch angle distributions were slightly lower at the equator, the behavior analyzed (i.e. higher energies associated with higher anisotropy) is unaffected by this shift.

## 6 Summary

In this study, we analyzed evolution of pitch angle distributions of relativistic and ultra relativistic electrons in geomagnetic storms with enhancements in the ultra relativistic energy range. The study investigated the temporal evolution of pitch angle indices obtained from fitting PADs of electrons spanning energy ranges from 1.8 to 7.7 MeV for individual storms with the functional form  $\sin^n(\theta)$ . The results of this study indicated that within storms, electron pitch angle distributions vary nearly simultaneously across energy channels, from relativistic to ultra relativistic energies. That is, an increase in the pitch angle index at relativistic energies was reflected in the ultra relativistic energies, both both decreased in pitch angle indices at the same time, although ultra relativistic electrons always had more anisotropic PADs than relativistic electrons.

We also performed a superposed epoch analysis of electron pitch angle index and compared electrons of the same energy across different storms. We found that electrons exhibit pitch angle coherence over a wide range of energies, and that pitch angle distributions change in the same manner across energies. Pitch angles consistently became more anisotropic in the day following *Dst* minimum of each storm. They then became more isotropic in the following week, at rates that were different for CME- and CIR- driven storms. The results of this study indicate a remarkable coherence, and emphasizes that there is more work to be done in regards to understanding the energization of electrons in the outer radiation belt.

We also investigated the temporal evolution of electron PADs for solar driver dependence, i.e., CME- and CIR- driven geomagnetic storms. Storms driven by CMEs have more anisotropic pitch angle distributions in the day following *Dst* minimum, and more rapidly isotropize to prestorm values after a storm than do CIR-driven storms. However the overall temporal behavior is the same between the storm drivers. This is true across relativistic and ultra relativistic electrons, suggesting that both energy regimes are accelerated in the same manner.

In summary, we found that pitch angle distributions are energy dependent, and that consecutively higher energies are consistently more anisotropic after storm onset. We also found that pitch angle indices generally peak within a day of *Dst<sub>min</sub>* and isotropization back to prestorm values can be fit linearly. CME-driven storms are both more anisotropic and have faster rates of isotropization than do CIR-driven storms. These may be caused by wave-particle interactions or a combination of wave-particle interactions and inward radial diffusion, prominent during storm times.

## Acknowledgments

A list of storms used can be found in supporting information. Van Allen Probes data are publicly accessible at <https://rbspgway.jhuapl.edu> and <https://rbsp-ect.lanl.gov/rbsp-ect.php>. This research was supported by an appointment to the NASA Postdoctoral Program at the NASA Goddard Space Flight Center, administered by Universities Space Research Association under contract with NASA. Research was also supported by the International Space Science Institute's (ISSI) International Teams program.

## References

Baker, D. N., Higbie, P. R., Hones Jr., E. W., & Belian, R. D. (1978). High-



- resolution energetic particle measurements at 6.6 re 3. low-energy electron anisotropies and short-term substorm predictions. *Journal of Geophysical Research: Space Physics*, 83(A10), 4863-4868. Retrieved from <https://agupubs.onlinelibrary.wiley.com/doi/abs/10.1029/JA083iA10p04863> doi: 10.1029/JA083iA10p04863
- Baker, D. N., Jaynes, A. N., Li, X., Henderson, M. G., Kanekal, S. G., Reeves, G. D., ... Shprits, Y. Y. (2014). Gradual diffusion and punctuated phase space density enhancements of highly relativistic electrons: Van allen probes observations. *Geophysical Research Letters*, 41(5), 1351-1358. Retrieved from <https://agupubs.onlinelibrary.wiley.com/doi/abs/10.1002/2013GL058942> doi: 10.1002/2013GL058942
- Baker, D. N., Kanekal, S. G., Hoxie, V. C., Henderson, M. G., Li, X., Spence, H. E., ... Claudepierre, S. G. (2013). A long-lived relativistic electron storage ring embedded in earth's outer van allen belt. *Science*, 340(6129), 186-190. Retrieved from <https://science.sciencemag.org/content/340/6129/186> doi: 10.1126/science.1233518
- Baker, D. N., et al. (2012). The relativistic electron-proton telescope (rept) instrument on board the radiation belt storm probes (rbps) spacecraft: Characterization of earth's radiation belt high-energy particle populations. *Space Sci. Rev.*, 179, 1-4. doi: 10.1007/s11214-012-9950-9
- Bingham, S. T., Mouikis, C. G., Kistler, L. M., Boyd, A. J., Paulson, K., Farrugia, C. J., ... Kletzing, C. (2018). The outer radiation belt response to the storm time development of seed electrons and chorus wave activity during cme and cir driven storms. *Journal of Geophysical Research: Space Physics*, 123(12), 10,139-10,157. Retrieved from <https://agupubs.onlinelibrary.wiley.com/doi/abs/10.1029/2018JA025963> doi: 10.1029/2018JA025963
- Chen, Y., Friedel, R. H. W., Henderson, M. G., Claudepierre, S. G., Morley, S. K., & Spence, H. E. (2014). Repad: An empirical model of pitch angle distributions for energetic electrons in the earth's outer radiation belt. *Journal of Geophysical Research: Space Physics*, 119(3), 1693-1708. Retrieved from <https://agupubs.onlinelibrary.wiley.com/doi/abs/10.1002/2013JA019431> doi: 10.1002/2013JA019431
- Chen, Y., Reeves, G. D., & Friedel, R. H. W. (2007). The energization of relativistic electrons in the outer van allen radiation belt. *Nature Physics*, 3(9), 614-617. Retrieved from <https://doi.org/10.1038/nphys655> doi: 10.1038/nphys655
- Claudepierre, S. G., Elkington, S. R., & Wiltberger, M. (2008). Solar wind driving of magnetospheric ulf waves: Pulsations driven by velocity shear at the magnetopause. *Journal of Geophysical Research: Space Physics*, 113(A5). Retrieved from <https://agupubs.onlinelibrary.wiley.com/doi/abs/10.1029/2007JA012890> doi: 10.1029/2007JA012890
- Fennell, J. F., Roeder, J. L., Kurth, W. S., Henderson, M. G., Larsen, B. A., Hospodarsky, G., ... Reeves, G. D. (2014). Van allen probes observations of direct wave-particle interactions. *Geophysical Research Letters*, 41(6), 1869-1875. Retrieved from <https://agupubs.onlinelibrary.wiley.com/doi/abs/10.1002/2013GL059165> doi: 10.1002/2013GL059165
- Fu, S., Ni, B., Lou, Y., Bortnik, J., Ge, Y., Tao, X., ... Wang, Q. (2018). Resonant scattering of near-equatorially mirroring electrons by landau resonance with h+ band emic waves. *Geophysical Research Letters*, 45(20), 10,866-10,873. Retrieved from <https://agupubs.onlinelibrary.wiley.com/doi/abs/10.1029/2018GL079718> doi: 10.1029/2018GL079718
- Fu, S., Yi, J., Ni, B., Zhou, R., Hu, Z., Cao, X., ... Guo, D. (2020). Combined scattering of radiation belt electrons by low-frequency hiss: Cyclotron, landau, and bounce resonances. *Geophysical Research Letters*, 47(5), e2020GL086963. Retrieved from <https://agupubs.onlinelibrary.wiley.com/doi/abs/>

- 10.1029/2020GL086963 (e2020GL086963 2020GL086963) doi: 10.1029/2020GL086963
- Gannon, J. L., et al. (2007). Pitch angle distribution analysis of radiation belt electrons based on combined release and radiation effects satellite medium electrons a data. *J. Geophys. Res: Space Physics*, 112(A5). Retrieved from <https://agupubs.onlinelibrary.wiley.com/doi/abs/10.1029/2005JA011565> doi: 10.1029/2005JA011565
- Geospace exploration project erg. (2018). *Earth, Planets and Space*, 70(1), 101. Retrieved from <https://doi.org/10.1186/s40623-018-0862-0> doi: 10.1186/s40623-018-0862-0
- Horne, R. B., et al. (2003). Evolution of energetic electron pitch angle distributions during storm time electron acceleration to megaelectronvolt energies. *J. Geophys. Res: Space Physics*, 108(A1), SMP 11-1-SMP 11-13. Retrieved from <https://agupubs.onlinelibrary.wiley.com/doi/abs/10.1029/2001JA009165> doi: 10.1029/2001JA009165
- Jaynes, A. N., Ali, A. F., Elkington, S. R., Malaspina, D. M., Baker, D. N., Li, X., ... Wygant, J. R. (2018). Fast diffusion of ultrarelativistic electrons in the outer radiation belt: 17 march 2015 storm event. *Geophysical Research Letters*, 45(20), 10,874-10,882. Retrieved from <https://agupubs.onlinelibrary.wiley.com/doi/abs/10.1029/2018GL079786> doi: 10.1029/2018GL079786
- Jaynes, A. N., Baker, D. N., Singer, H. J., Rodriguez, J. V., Loto'aniu, T. M., Ali, A. F., ... Reeves, G. D. (2015). Source and seed populations for relativistic electrons: Their roles in radiation belt changes. *Journal of Geophysical Research: Space Physics*, 120(9), 7240-7254. Retrieved from <https://agupubs.onlinelibrary.wiley.com/doi/abs/10.1002/2015JA021234> doi: 10.1002/2015JA021234
- Jian, L. (1993). *Radial evolution of large?scale solar wind structures* (Unpublished doctoral dissertation). Univ. of Calif., Los Angeles.
- Jordanova, V. K., Farrugia, C. J., Thorne, R. M., Khazanov, G. V., Reeves, G. D., & Thomsen, M. F. (n.d.). Modeling ring current proton precipitation by electromagnetic ion cyclotron waves during the may 14-16, 1997, storm. *Journal of Geophysical Research: Space Physics*, 106(A1), 7-22. Retrieved from <https://agupubs.onlinelibrary.wiley.com/doi/abs/10.1029/2000JA002008> doi: 10.1029/2000JA002008
- Kanekal, S. G. (2006). A review of recent observations of relativistic electron energization in the Earth's outer Van Allen radiation belt. In N. Gopalswamy & A. Bhattacharyya (Eds.), *Proceedings of the ilws workshop* (p. 274).
- Kanekal, S. G., Baker, D. N., & Blake, J. B. (2001). Multisatellite measurements of relativistic electrons: Global coherence. *Journal of Geophysical Research: Space Physics*, 106(A12), 29721-29732. Retrieved from <https://agupubs.onlinelibrary.wiley.com/doi/abs/10.1029/2001JA000070> doi: 10.1029/2001JA000070
- Kanekal, S. G., Baker, D. N., Blake, J. B., Klecker, B., Mewaldt, R. A., & Mason, G. M. (1999, November). Magnetospheric response to magnetic cloud (coronal mass ejection) events: Relativistic electron observations from SAMPEX and Polar. *Journal of Geophysics Research*, 104, 24885-24894. doi: 10.1029/1999JA900239
- Kanekal, S. G., Friedel, R. H. W., Reeves, G. D., Baker, D. N., & Blake, J. B. (2005). Relativistic electron events in 2002: Studies of pitch angle isotropization. *Journal of Geophysical Research: Space Physics*, 110(A12). Retrieved from <https://agupubs.onlinelibrary.wiley.com/doi/abs/10.1029/2004JA010974> doi: 10.1029/2004JA010974
- Kasahara, S., Miyoshi, Y., Yokota, S., Mitani, T., Kasahara, Y., Matsuda, S., ... Shinohara, I. (2018). Pulsating aurora from electron scattering by chorus

- 554 waves. *Nature*, 554(7692), 337–340. Retrieved from [https://doi.org/](https://doi.org/10.1038/nature25505)  
555 10.1038/nature25505 doi: 10.1038/nature25505
- 556 Lejosne, S., & Kollmann, P. (2020). Radiation belt radial diffusion at earth and be-  
557 yond. *Space Science Reviews*, 216(1), 19. Retrieved from [https://doi.org/](https://doi.org/10.1007/s11214-020-0642-6)  
558 10.1007/s11214-020-0642-6 doi: 10.1007/s11214-020-0642-6
- 559 Lyons, L. R., & Williams, D. J. (1975). The storm and poststorm evolution of  
560 energetic (35–560 keV) radiation belt electron distributions. *J. Geophys. Res.*,  
561 80(28), 3985–3994. Retrieved from [https://agupubs.onlinelibrary.wiley](https://agupubs.onlinelibrary.wiley.com/doi/abs/10.1029/JA080i028p03985)  
562 .com/doi/abs/10.1029/JA080i028p03985 doi: 10.1029/JA080i028p03985
- 563 Mauk, B. H., Fox, N. J., Kanekal, S. G., Kessel, R. L., Sibeck, D. G., & Ukhorskiy,  
564 A. (2013, Nov 01). Science objectives and rationale for the radiation  
565 belt storm probes mission. *Space Science Reviews*, 179(1), 3–27. Re-  
566 trieved from <https://doi.org/10.1007/s11214-012-9908-y> doi:  
567 10.1007/s11214-012-9908-y
- 568 Meredith, N. P., Thorne, R. M., Horne, R. B., Summers, D., Fraser, B. J., & An-  
569 derson, R. R. (2003). Statistical analysis of relativistic electron energies  
570 for cyclotron resonance with emic waves observed on crres. *Journal of*  
571 *Geophysical Research: Space Physics*, 108(A6). Retrieved from [https://](https://agupubs.onlinelibrary.wiley.com/doi/abs/10.1029/2002JA009700)  
572 agupubs.onlinelibrary.wiley.com/doi/abs/10.1029/2002JA009700 doi:  
573 10.1029/2002JA009700
- 574 Mourenas, D., Artemyev, A. V., Agapitov, O. V., & Krasnoselskikh, V. (2014).  
575 Consequences of geomagnetic activity on energization and loss of radia-  
576 tion belt electrons by oblique chorus waves. *Journal of Geophysical Re-*  
577 *search: Space Physics*, 119(4), 2775–2796. Retrieved from [https://](https://agupubs.onlinelibrary.wiley.com/doi/abs/10.1002/2013JA019674)  
578 agupubs.onlinelibrary.wiley.com/doi/abs/10.1002/2013JA019674 doi:  
579 10.1002/2013JA019674
- 580 Neugebauer, M., & Goldstein, R. (2013). Particle and field signatures of coro-  
581 nal mass ejections in the solar wind. In *Coronal mass ejections* (p. 245-  
582 251). American Geophysical Union (AGU). Retrieved from [https://](https://agupubs.onlinelibrary.wiley.com/doi/abs/10.1029/GM099p0245)  
583 agupubs.onlinelibrary.wiley.com/doi/abs/10.1029/GM099p0245 doi:  
584 10.1029/GM099p0245
- 585 Ni, B., et al. (2015). Variability of the pitch angle distribution of radiation belt  
586 ultrarelativistic electrons during and following intense geomagnetic storms:  
587 Van allen probes observations. *J. Geophys. Res: Space Physics*, 120(6), 4863-  
588 4876. Retrieved from [https://agupubs.onlinelibrary.wiley.com/doi/abs/](https://agupubs.onlinelibrary.wiley.com/doi/abs/10.1002/2015JA021065)  
589 10.1002/2015JA021065 doi: 10.1002/2015JA021065
- 590 O'Brien, T. P., Lorentzen, K. R., Mann, I. R., Meredith, N. P., Blake, J. B., Fen-  
591 nell, J. F., ... Anderson, R. R. (2003). Energization of relativistic electrons  
592 in the presence of ulf power and mev microbursts: Evidence for dual ulf and  
593 vlf acceleration. *Journal of Geophysical Research: Space Physics*, 108(A8).  
594 Retrieved from [https://agupubs.onlinelibrary.wiley.com/doi/abs/](https://agupubs.onlinelibrary.wiley.com/doi/abs/10.1029/2002JA009784)  
595 10.1029/2002JA009784 doi: 10.1029/2002JA009784
- 596 Reeves, G., Cayton, T., Friedel, R., Jahn, J., Henderson, M., Meier, M., ... others  
597 (1998). Relativistic electron observations in the three-dimensional magneto-  
598 sphere. *Eos Trans, AGU*, 79, 17.
- 599 Reeves, G. D., McAdams, K. L., Friedel, R. H. W., & O'Brien, T. P. (2003).  
600 Acceleration and loss of relativistic electrons during geomagnetic storms.  
601 *Geophysical Research Letters*, 30(10). Retrieved from [https://agupubs](https://agupubs.onlinelibrary.wiley.com/doi/abs/10.1029/2002GL016513)  
602 .onlinelibrary.wiley.com/doi/abs/10.1029/2002GL016513 doi:  
603 10.1029/2002GL016513
- 604 Reeves, G. D., Spence, H. E., Henderson, M. G., Morley, S. K., Friedel, R. H. W.,  
605 Funsten, H. O., ... Niehof, J. T. (2013). Electron acceleration in the heart  
606 of the van allen radiation belts. *Science*, 341(6149), 991–994. Retrieved  
607 from <https://science.sciencemag.org/content/341/6149/991> doi:  
608 10.1126/science.1237743

- Richardson, I., & Cane, H. (2019). *Near-earth interplanetary coronal mass ejections since january 1996*. Retrieved 2019-08-28, from <http://www.srl.caltech.edu/ACE/ASC/DATA/level3/icmetable2.htm>
- Selesnick, R. S., & Blake, J. B. (2002). Relativistic electron drift shell splitting. *J. Geophys. Res: Space Physics*, 107(A9), SMP 27-1-SMP 27-10. Retrieved from <https://agupubs.onlinelibrary.wiley.com/doi/abs/10.1029/2001JA009179> doi: 10.1029/2001JA009179
- Shen, X., Hudson, M. K., Jaynes, A. N., Shi, Q., Tian, A., Claudepierre, S. G., ... Sun, W. (2017, 8). Statistical study of the storm time radiation belt evolution during van allen probes era: Cme- versus cir-driven storms. *Journal of Geophysical Research: Space Physics*, 122(8), 8327–8339. Retrieved from <https://doi.org/10.1002/2017JA024100> doi: 10.1002/2017JA024100
- Shprits, Y. Y. (2009). Potential waves for pitch-angle scattering of near-equatorially mirroring energetic electrons due to the violation of the second adiabatic invariant. *Geophysical Research Letters*, 36(12). Retrieved from <https://agupubs.onlinelibrary.wiley.com/doi/abs/10.1029/2009GL038322> doi: 10.1029/2009GL038322
- Sibeck, D., Kanekal, S., Fox, N., Mauk, B., & Kessel, R. (2012, 07). The radiation belt storm probes mission: Advancing our understanding of the earth's radiation belts. , 1806-.
- Sibeck, D. G., et al. (1987). Magnetic field drift shell splitting: Cause of unusual dayside particle pitch angle distributions during storms and substorms. *J. Geophys. Res: Space Physics*, 92(A12), 13485-13497. Retrieved from <https://agupubs.onlinelibrary.wiley.com/doi/abs/10.1029/JA092iA12p13485> doi: 10.1029/JA092iA12p13485
- Stone, E. C. (1963). The physical significance and application of  $l$ ,  $b_0$ , and  $r_0$  to geomagnetically trapped particles. *J. Geophys. Res*, 68(14), 4157-4166.
- Summers, D., & Thorne, R. M. (2003). Relativistic electron pitch-angle scattering by electromagnetic ion cyclotron waves during geomagnetic storms. *Journal of Geophysical Research: Space Physics*, 108(A4). Retrieved from <https://agupubs.onlinelibrary.wiley.com/doi/abs/10.1029/2002JA009489> doi: 10.1029/2002JA009489
- Summers, D., Thorne, R. M., & Xiao, F. (1998). Relativistic theory of wave-particle resonant diffusion with application to electron acceleration in the magnetosphere. *Journal of Geophysical Research: Space Physics*, 103(A9), 20487-20500. Retrieved from <https://agupubs.onlinelibrary.wiley.com/doi/abs/10.1029/98JA01740> doi: 10.1029/98JA01740
- Thorne, R. M. (2010). Radiation belt dynamics: The importance of wave-particle interactions. *Geophysical Research Letters*, 37(22). Retrieved from <https://agupubs.onlinelibrary.wiley.com/doi/abs/10.1029/2010GL044990> doi: 10.1029/2010GL044990
- Thorne, R. M., Li, W., Ni, B., Ma, Q., Bortnik, J., Baker, D. N., ... Angelopoulos, V. (2013). Evolution and slow decay of an unusual narrow ring of relativistic electrons near  $l \approx 3.2$  following the september 2012 magnetic storm. *Geophysical Research Letters*, 40(14), 3507-3511. Retrieved from <https://agupubs.onlinelibrary.wiley.com/doi/abs/10.1002/grl.50627> doi: 10.1002/grl.50627
- Thorne, R. M., Li, W., Ni, B., Ma, Q., Bortnik, J., Chen, L., ... Kanekal, S. G. (2013). Rapid local acceleration of relativistic radiation-belt electrons by magnetospheric chorus. *Nature*, 504(7480), 411–414. Retrieved from <https://doi.org/10.1038/nature12889> doi: 10.1038/nature12889
- Turner, D. L., O'Brien, T. P., Fennell, J. F., Claudepierre, S. G., Blake, J. B., Kilpua, E. K. J., & Hietala, H. (2015). The effects of geomagnetic storms on electrons in earth's radiation belts. *Geophysical Research Letters*, 42(21), 9176-9184. Retrieved from <https://agupubs.onlinelibrary.wiley.com/>

- doi/abs/10.1002/2015GL064747 doi: 10.1002/2015GL064747
- Wang, B., Su, Z., Zhang, Y., Shi, S., & Wang, G. (2016). Nonlinear landau resonant scattering of near equatorially mirroring radiation belt electrons by oblique emic waves. *Geophysical Research Letters*, 43(8), 3628-3636. Retrieved from <https://agupubs.onlinelibrary.wiley.com/doi/abs/10.1002/2016GL068467> doi: 10.1002/2016GL068467
- West Jr., H. I., et al. (1973). Electron pitch angle distributions throughout the magnetosphere as observed on ogo 5. *J. Geophys. Res*, 78(7), 1064-1081. Retrieved from <https://agupubs.onlinelibrary.wiley.com/doi/abs/10.1029/JA078i007p01064> doi: 10.1029/JA078i007p01064
- Zhao, H., Baker, D., Li, X., Malaspina, D., Jaynes, A., & Kanekal, S. (2019). On the acceleration mechanism of ultrarelativistic electrons in the center of the outer radiation belt: A statistical study. *Journal of Geophysical Research: Space Physics*, 124(11), 8590-8599. Retrieved from <https://agupubs.onlinelibrary.wiley.com/doi/abs/10.1029/2019JA027111> doi: 10.1029/2019JA027111
- Zhao, H., Li, X., Blake, J. B., Fennell, J. F., Claudepierre, S. G., Baker, D. N., ... Kanekal, S. G. (2014). Peculiar pitch angle distribution of relativistic electrons in the inner radiation belt and slot region. *Geophysical Research Letters*, 41(7), 2250-2257. Retrieved from <https://agupubs.onlinelibrary.wiley.com/doi/abs/10.1002/2014GL059725> doi: 10.1002/2014GL059725
- Zhao, H., et al. (2018). An empirical model of radiation belt electron pitch angle distributions based on van allen probes measurements. *J. Geophys. Res: Space Physics*, 123(5), 3493-3511. Retrieved from <https://agupubs.onlinelibrary.wiley.com/doi/abs/10.1029/2018JA025277> doi: 10.1029/2018JA025277
- Zhao, H., et al. (2019). The effects of geomagnetic storms and solar wind conditions on the ultrarelativistic electron flux enhancements. *J. Geophys. Res: Space Physics*, 124(3), 1948-1965. Retrieved from <https://agupubs.onlinelibrary.wiley.com/doi/abs/10.1029/2018JA026257> doi: 10.1029/2018JA026257